

Protostellar Collapse Induced by Compression

P. Hennebelle,^{1*} A. P. Whitworth,^{1†} P. P. Gladwin,¹ Ph. André,^{2‡}

¹*Department of Physics & Astronomy, Cardiff University, PO Box 913, 5 The Parade, Cardiff CF24 3YB, Wales, UK*

²*CEA, DSM, DAPNIA, Service d'Astrophysique, C. E. Saclay, F-91191 Gif-sur-Yvette Cedex, France*

Accepted. Received; in original form

ABSTRACT

We present numerical simulations of the evolution of low-mass, isothermal, molecular cores which are subjected to an increase in external pressure P_{ext} . If P_{ext} increases very slowly, the core approaches instability quite quasistatically. However, for larger (but still quite modest) dP_{ext}/dt a compression wave is driven into the core, thereby triggering collapse from the outside in. If collapse of a core is induced by increasing P_{ext} , this has a number of interesting consequences. (i) The density profile is approximately flat in the centre during the prestellar phase (i.e. before the compression wave converges on the centre creating the central protostar). (ii) During the prestellar phase there are (subsonic) inward velocities in the outer layers of the core, whilst the inner parts are still approximately at rest. (iii) There is an initial short phase of rapid accretion (notionally the Class 0 phase), followed by a longer phase of slower accretion (the Class I phase). All these features accord well with observation, but are at variance with the predictions of the standard theory of star formation based on the inside-out collapse of a singular isothermal sphere. We note that the setting up of a coherent inward velocity field appears to be a generic feature of compression waves; and we speculate that interactions and interference between such velocity fields may play a crucial rôle in initiating the fragmentation of cores and the genesis of multiple star systems.

Key words: stars: formation.

1 INTRODUCTION

The initial conditions for star formation are in general rather weakly constrained. The observations (e.g. André, Ward-Thompson, & Barsony 2000; Myers, Evans, & Ohashi 2000) are limited by telescope resolution and confusion, and their interpretation is hindered by the complexities and uncertainties of gas-phase abundances, excitation conditions, and radiation transport. However, a picture is emerging which suggests that star formation is sometimes triggered rather impulsively.

Molecular-line mapping by Myers and collaborators (e.g. Myers & Benson 1983; Benson & Myers 1989) and subsequent searches by Clemens & Barvainis (1988), Bourke, Hyland & Robinson (1995), Jessop & Ward-Thompson (2000), have established a large sample of dense cores which appear to be the sites of ongoing or imminent star formation. Many of these cores contain IRAS sources (Beichman et al.

1986), and are therefore presumed to have already formed protostars. Those which do not contain IRAS sources are termed starless cores.

Submillimeter mapping of these starless cores by Ward-Thompson et al. (1994, 1999) has identified a subset which, on the basis of their virial ratios and relatively high central densities, are likely to be in a state of imminent or ongoing contraction. These starless cores are therefore termed prestellar (strictly pre-protostellar). Submillimeter mapping of prestellar cores (Ward-Thompson et al. 1994, André et al. 1996, Ward-Thompson et al. 1999) suggests that, if the emitting dust is isothermal, the cores have rather flat density profiles in the centre. Specifically, $\eta \equiv -d\ln[\rho]/d\ln[r]$ is in the range 0 to 1, in the innermost few thousand AU. This conclusion may be somewhat weaker if, as seems likely (Jessop & Ward-Thompson 2001; Evans et al. 2001; Zucconi, Walmsley & Galli 2001; Ward-Thompson, André & Kirk, 2001), the dust temperature decreases towards the centre of a core. However, mid-infrared absorption measurements of prestellar cores – which are insensitive to the temperature profile – also indicate flat inner density profiles (Bacmann et al. 2000). Additionally, mid-infrared observations suggest

* Patrick.Hennebelle@astro.cf.ac.uk

† ant@astro.cf.ac.uk

‡ pandre@discovery.saclay.cea.fr

that beyond $\sim 10,000$ AU the density profile may steepen to $\eta \gtrsim 4$ (Abergel et al. 1996, Bacmann et al. 2000). This steepening of the outer envelope appears to occur at smaller radii in relatively close-packed protoclusters like ρ Ophiuchi than in regions of distributed star formation such as Taurus; viz. at $\sim 3,000$ AU in ρ Ophiuchi, and at $\sim 15,000$ AU in Taurus (Motte & André 2001).

The asymmetric self-absorbed molecular-line profiles observed in some prestellar cores (Tafalla et al. 1998, Williams et al. 1999, Lee, Myers & Tafalla 1999, Gregersen & Evans 2000) suggest that they are indeed already collapsing. In particular, the detailed analyses of L1544 by Tafalla et al. (1998) and Williams et al. (1999) imply that the inner parts of the core are relatively stationary, and an approximately uniform velocity field has been established in the outer layers. This is very reminiscent of the velocity fields which are set up by inward-propagating compression waves in similarity solutions for contracting isothermal spheres (Whitworth & Summers 1985). It is this apparent similarity which we explore in the present paper.

The prestellar phase terminates as soon as a star-like object forms at the centre of the dense core, and the core then becomes a Class 0 protostar. Conceptually, the Class 0 protostellar phase terminates once the extended envelope contains less than half the total mass of the original core, i.e. more than half the mass is in the central star-like object(s) plus attendant disc(s) (André, Ward-Thompson & Barsony 1993, 2000); the Class I phase then begins (Lada & Wilking 1984, Lada 1987, André & Montmerle 1994). The Class I protostellar phase terminates when most of the envelope has been accreted or dissipated, revealing a classical T Tauri star (CTTS) accreting from a residual circumstellar disc, i.e. a Class II object. Once the inner disc has been dissipated, the accretion rate is greatly reduced and the source becomes a weak-lined T Tauri star (WTTS) or Class III object.

On the basis of statistical arguments (i.e. source numbers and a presumed constant star formation rate) it is inferred (Beichmann et al. 1986, André, Ward-Thompson & Barsony 2000) that the prestellar phase lasts, typically, 10^6 to 10^7 years. In close-packed protoclusters like ρ Ophiuchi, the Class 0 phase appears to last a few times 10^4 years, and is characterized by powerful collimated outflows indicative of rapid accretion, $\gtrsim 10^{-5} M_{\odot} \text{ year}^{-1}$ (Bontemps et al. 1996). In distributed star formation regions like Taurus, the duration of the Class 0 phase appears to be longer, $\sim 10^5$ years, and the accretion rates lower, $\gtrsim 2 \times 10^{-6} M_{\odot} \text{ year}^{-1}$ (Motte & André 2001). The Class I phase appears to last $\sim 2 \times 10^5$ years (e.g. Greene et al. 1994, Kenyon & Hartmann 1995) and is characterized by slower accretion, $\lesssim 10^{-6} M_{\odot} \text{ year}^{-1}$, and weaker less collimated outflows (Bontemps et al. 1996). Together, the Class II and Class III phases appear to last $\gtrsim 10^7$ years, but seemingly the transition from Class II (CTTS) to Class III (WTTS) is very short and can occur at any time; there are both very young WTTSs (close to the birthline, on the right of the Hertzsprung-Russell Diagram) and very old CTTSs (approaching the Main Sequence on the left of the Hertzsprung-Russell Diagram) (e.g. Stahler & Walter 1993).

These observationally inferred features of prestellar and protostellar evolution combine to form a reasonably coherent picture. However, especially in star-forming clusters, this picture is difficult to reconcile with the standard the-

ory of Shu, Adams & Lizano (1987) based on the inside-out collapse of a singular isothermal sphere. The strength of the standard theory is that it makes specific quantitative predictions, but some of these predictions are difficult to reconcile with observation. (i) In the standard model, prestellar cores should be strongly centrally condensed, $\eta \equiv -d\ln[\rho]/d\ln[r] \sim 2$ and young protostars should be somewhat less centrally condensed, $\eta \sim 3/2$. By contrast, observations suggest that prestellar cores have rather flat central density profiles, $\eta \lesssim 1$, and Class 0 protostars have steeper ones. (ii) The standard theory predicts that prestellar cores are static, and that inward motions only develop during the protostellar phase and are initially confined to the central regions. In contrast, the observations imply that inward motions already exist during the prestellar phase, and that initially they are more rapid in the outer regions. (iii) The standard theory predicts that the accretion rate is roughly constant, and hence the Class 0 and Class I lifetimes should be comparable. Observations detect many more Class I sources than Class 0 ones – although this statistical result may be compromised by the difficulty of measuring precisely when an object has accreted half the total mass of its initial core. (iv) Additionally, the standard theory assumes initial conditions which are unlikely to arise in nature, because they are both singular and unstable. (v) Also the standard theory has a strong inbuilt pre-disposition to the formation of single stars – in stark contrast with the high proportion of binaries and higher multiples observed in young star-formation regions. Therefore, although the standard theory may provide a good, zeroth-order description of protostellar collapse in sparse, quiescent star-formation regions like Taurus (cf. Motte & André 2001), it appears that more dynamical models are required to understand close-packed regions like ρ Ophiuchi.

Foster & Chevalier (1993) have explored how the collapse of an isothermal core develops if one abandons the assumption of singularity. Their simulations start from non-singular isothermal equilibria, i.e. Bonnor-Ebert spheres (e.g. Bonnor 1956), and collapse is then triggered by discontinuously increasing the density. The ensuing collapse results in supersonic inflow velocities in the centre of the core at the end of the prestellar phase, and in a marked decline of the accretion rate from the Class 0 to the Class I phase (see Henriksen, André, Bontemps 1997 and Whitworth & Ward-Thompson 2001 for simpler, pressure-free descriptions of this evolution).

In this paper we pursue the consequences of non-singularity further. Our simulations also start from non-singular isothermal equilibrium cores, but collapse is then triggered by a steady increase in the external pressure (cf. Myers & Lazarian 1998). Most of the observational constraints detailed above can be reproduced rather well by this model.

In Section 2 we describe the numerical method we use, and the initial and boundary conditions. In Section 3 we present the results, and in Section 4 we discuss them. Section 5 summarizes our main conclusions.

2 NUMERICAL METHOD

The simulations are performed using a Smoothed Particle Hydrodynamics code – essentially that described in Turner et al. (1995). We use the B2-spline smoothing kernel of Monaghan & Lattanzio (1985),

$$W(s) = \frac{1}{4\pi} \begin{cases} 4 - 6s^2 + 3s^3, & 0 \leq s \leq 1; \\ (2 - s)^3, & 1 < s \leq 2; \\ 0, & s > 2. \end{cases} \quad (1)$$

and the smoothing lengths of the individual particles are adjusted so that the kernel encompasses $\mathcal{N}_{\text{neib}} \simeq 50 \pm 5$ neighbours, i.e. for particle i the smoothing length h_i is adjusted so that there are $\mathcal{N}_{\text{neib}}$ other particles j having

$$|\mathbf{r}_j - \mathbf{r}_i| < 2\bar{h}_{ij} \equiv h_i + h_j. \quad (2)$$

If we define $\Delta\mathbf{v}_{ij} \equiv \mathbf{v}_i - \mathbf{v}_j$; $\Delta\mathbf{r}_{ij} \equiv \mathbf{r}_i - \mathbf{r}_j$; $\bar{a}_{ij} \equiv 0.5(a_i + a_j)$; $\bar{\rho}_{ij} \equiv 0.5(\rho_i + \rho_j)$;

$$\Pi_{ij} = \frac{-\alpha\mu_{ij}\bar{a}_{ij} + \beta\mu_{ij}^2}{\bar{\rho}_{ij}},$$

$$\mu_{ij} = \begin{cases} \bar{h}_{ij}\mathbf{v}_{ij}\cdot\mathbf{r}_{ij} (|\mathbf{r}_{ij}|^2 + \gamma\bar{h}_{ij}^2)^{-1}, & \mathbf{v}_{ij}\cdot\mathbf{r}_{ij} < 0, \\ 0, & \mathbf{v}_{ij}\cdot\mathbf{r}_{ij} > 0; \end{cases}$$

$W'(s) \equiv dW/ds$, and

$$W^*(s) = \int_{s'=0}^{s'=s} W(s') 4\pi s'^2 ds'; \quad (3)$$

then the equation of motion for particle i is

$$\frac{d\mathbf{v}_i}{dt} = - \sum_j \left\{ \frac{m_j}{\bar{h}_{ij}^4} \left[\frac{P_i}{\rho_i^2} + \frac{P_j}{\rho_j^2} + \Pi_{ij} \right] W' \left(\frac{|\Delta\mathbf{r}_{ij}|}{\bar{h}_{ij}} \right) \frac{\Delta\mathbf{r}_{ij}}{|\Delta\mathbf{r}_{ij}|} \right\} - \sum_{j'} \left\{ m_{j'} W^* \left(\frac{|\Delta\mathbf{r}_{ij'}|}{\bar{h}_{ij'}} \right) \frac{\Delta\mathbf{r}_{ij'}}{|\Delta\mathbf{r}_{ij'}|^3} \right\}. \quad (4)$$

The first summation determines the hydrostatic and viscous accelerations. Since $W'(s) = 0$ for $s > 2$, this summation only extends over neighbours, i.e. particles satisfying Eqn. (2). Π_{ij} is the artificial viscosity term and acts only between neighbours which are approaching one another. We use $\alpha = 1$, $\beta = 2$, and $\gamma = 0.01$.

The second summation determines the gravitational acceleration. Since $W^*(s) > 0$ for all $s > 0$, this summation extends over all particles. The gravitational attraction between particles whose kernels overlap is softened by $W^*(s)$, in accordance with Gauss's Gravitational Theorem; implicitly the gravitational softening length and the hydrostatic smoothing length are the same, as advocated by Bate & Burkert (1997). We use an octal spatial tessellation tree (Barnes & Hut 1986, Hernquist 1987) to find neighbours, and also to speed up the calculation of gravity. Thus in the second summation in Eqn. (4) j' may represent the identifier of an individual particle or a cell in the tree. To evaluate this sum, the tree is walked from the root cell (representing the whole computational domain) downwards. Whenever a cell j' is encountered which satisfies the non-opening condition

$$L_{j'} < \theta_{\text{crit}} |\mathbf{r}_i - \mathbf{R}_{j'}|, \quad (5)$$

that cell contributes to the sum as a point mass, and all smaller cells and individual particles within that cell can be neglected. In Eqn. (5), $L_{j'}$ is the linear size of the cell under consideration, $\mathbf{R}_{j'}$ is the position of the cell's centre of mass, and θ_{crit} is the maximum opening angle which a cell can subtend at particle i without being opened. We use $\theta_{\text{crit}} = 3^{-1/2} \simeq 0.577$.

The density at particle i is given by

$$\rho_i = \sum_j \left\{ \frac{m_j}{\bar{h}_{ij}^3} W \left(\frac{|\Delta\mathbf{r}_{ij}|}{\bar{h}_{ij}} \right) \right\}. \quad (6)$$

We use an isothermal equation of state

$$a_i = a_o, \quad P_i = a_o^2 \rho_i, \quad (7)$$

and so we do not need to solve an energy equation.

The code uses multiple-particle time-steps,

$$\Delta t_n = \Delta t_o 2^n, \quad n = 0, 1, 2, \dots, n_{\text{max}}. \quad (8)$$

The maximum possible time-step for each particle is given by

$$\Delta t_i^{\text{max}} = \delta \text{MIN} \left\{ \frac{1}{|\nabla\cdot\mathbf{v}|_i}, \frac{h_i}{|\mathbf{v}_i|}, \left(\frac{h_i}{|\mathbf{a}_i|} \right)^{1/2}, \frac{h_i}{(2.2 c_i + 1.2 \text{MAX}_j \{\mu_{ij}\})} \right\}. \quad (9)$$

Then each particle i is allocated the largest Δt_n which is smaller than Δt_i^{max} , i.e. Δt_{n_i} with

$$n_i = \text{INT} \left\{ \frac{\log[\Delta t_i^{\text{max}}/\Delta t_o]}{\log[2]} \right\}, \quad (10)$$

with the additional proviso that the current time-step must be an integer multiple of Δt_{n_i} .

At the start of a simulation, cores are modelled as truncated equilibrium isothermal spheres, contained by a hot rarefied external medium. These initial conditions are realized by distributing particles randomly in a cubic box with periodic boundary conditions, and settling them using SPH forces only (i.e. the terms in the first summation in Eqn. (4)); this creates a uniform-density settled cube. Next a sphere is cut from the settled cube, and the particle positions within the sphere are stretched radially to reproduce the density profile of a truncated isothermal sphere. Isothermal spheres having different degrees of central condensation are created by picking different values of $\xi_b = R_o (4\pi G \rho_c)^{1/2} a_o^{-1}$, where ξ_b is the dimensionless radius of a truncated equilibrium isothermal sphere, R_o is the physical radius of the core (*not* the scale-length), and ρ_c is the central density in the core. Stability requires $\xi_b < 6.45$ (Bonnor 1956).

The particles inside the sphere are then tagged as being *internal* particles, and henceforth they experience both SPH forces and mutual gravity, i.e. they are evolved using both the summations in Eqn. (4). The particles outside the sphere are tagged as *external* particles, and henceforth they are evolved using only SPH forces, i.e. only the first summation in Eqn. (4). The external particles are given whatever sound speed is needed for them to deliver the prescribed external pressure $P_{\text{ext}}(t)$ at the edge of the sphere,

i.e. $a_i(t) = (P_{\text{ext}}(t)/\rho_i(t))^{1/2}$. In addition, there is a layer of fixed *edge* particles at the boundary of the computational domain. These fixed edge particles have constant density ρ_{edge} and they are not evolved, but they exert SPH forces on the external particles and their sound speed is given by $a_{\text{edge}} = (P_{\text{ext}}(t)/\rho_{\text{edge}})^{1/2}$.

At the outset, the sphere is relaxed with P_{ext} held constant, so that it can settle to equilibrium. There is some variance between the true isothermal sphere characterized by the chosen value of ξ_b and the actual SPH-modelled configuration, due to the density smoothing at the core boundary, where the density gradient is steep. This leads to an effective external pressure which is a little higher than the specified one. The only significant consequence of this is that the onset of collapse is somewhat accelerated in the case of slow compression ($\phi = 10$). This is due to transient oscillations which for slow compression have time to propagate inwards from the boundary and increase the density at the centre.

Stable equilibrium isothermal spheres constructed in this way are then subjected to increasing external pressure. For simplicity we prescribe

$$P_{\text{ext}}(t > 0) = P_{\text{ext}}(0) + \dot{P}_o t, \quad (11)$$

with constant \dot{P}_o . Rather than give \dot{P}_o in physical units, we define a dimensionless parameter

$$\phi = \frac{P_{\text{ext}}(0)/\dot{P}_o}{R_o/a_o}, \quad (12)$$

which is the ratio of the time-scale on which the external pressure doubles to the initial sound-crossing time (R_o is the initial radius of the core). Small \dot{P}_o corresponds to large ϕ . Simulations have been performed with a variety of ϕ values between $\phi = 10$ (very slow compression) and $\phi = 0.1$ (very fast compression).

There is a simple spherical sink at the centre of the core, having radius 150 AU (i.e. $\sim 1\%$ of the initial core radius), and representing the central protostar (plus attendant disc). Any particle entering the sink is assimilated by it. The protostar is assumed to come into existence as soon as the sink starts to gain mass. Hence we can easily compute its mass and accretion rate, as functions of time.

We fix the core mass at $M_o = 1 M_\odot$, the sound speed in the core at $a_o = 0.2 \text{ km s}^{-1}$ (corresponding to a cosmic mixture of molecular hydrogen, helium and heavy elements at $\sim 10 \text{ K}$), and the stability parameter of the initial core at $\xi_b = 3.0$. The radius of the core is initially $\sim 0.08 \text{ pc}$. The standard simulations presented in the next section are performed with $\mathcal{N}_{\text{int}} \sim 50,000$ internal particles, $\mathcal{N}_{\text{ext}} \sim 25,000$ external particles, and $\mathcal{N}_{\text{edge}} \sim 20,000$ edge particles; some simulations with fewer particles have been performed to demonstrate convergence.

3 RESULTS

Figure 1 shows detailed results for the $\phi = 10$ case (i.e. very slow compression; P_{ext} takes ten sound-crossing times to double). In this case the evolution towards gravitational instability is relatively quasistatic, because there is time for sound waves to slop around re-distributing the matter. During the prestellar phase (the first three rows on

Fig. 1), the outer boundary is pushed inwards, and the core becomes increasingly centrally condensed; the outer parts of the core move slowly inwards at speeds up to $\sim 0.03 \text{ km s}^{-1}$ ($\equiv 0.15 a_o$), whilst matter near the centre is approximately stationary. Eventually the core becomes unstable and collapses; this is the start of the Class 0 phase. At this stage the radius of the core is $\sim 0.06 \text{ pc}$. As the subsequent collapse proceeds, a freefall velocity field ($v \propto r^{-1/2}$) develops from the inside out, steadily replacing the more modest approximately uniform velocity field in the outer layers (the fourth and fifth rows on Fig. 1). The rate of accretion onto the central protostar (sink) is quite modest, with a maximum value $\sim 0.65 \times 10^{-5} M_\odot \text{ yr}^{-1}$, after which it decreases steadily into the Class I phase. The evolution of the sink mass and the accretion rate is shown on the first row of Fig. 7. The durations of the prestellar and Class 0 phases are given in Table 1, along with an estimate of the mean cruising velocity set up by the passage of the compression wave.

This case is the one closest to the standard case of Foster & Chevalier (1993). In their simulation collapse was initiated by taking a marginally unstable (i.e. critical) Bonnor-Ebert sphere and increasing the density by 10%. As a result, contraction was driven by an imbalance between self-gravity and pressure. Immediately following the formation of the central protostar the accretion rate was very high, and subsequently it decreased. In the $\phi = 10$ case here, contraction is driven by compression, and when the resulting compression wave converges on the centre the accretion rate builds up to a maximum somewhat more slowly (than in Foster and Chevalier's simulation). In both cases the maximum accretion rate occurs during the Class 0 phase, and is significantly larger than the standard $\dot{M} \sim a_o^3/G \sim 2 \times 10^{-6} M_\odot \text{ year}^{-1}$.

Figure 2 shows the case $\phi = 3$ (i.e. quite slow compression; P_{ext} doubles in 3 sound-crossing times). The evolution is somewhat less quasistatic (than for $\phi = 10$, Fig. 1), but basically it is very similar. The outer boundary is pushed inwards, and the core becomes steadily more centrally condensed throughout the prestellar phase (the first three rows of Fig. 2); the outer layers start to move inwards at speeds in the range $(0.05, 0.07) \text{ km s}^{-1}$, whilst matter near the centre is approximately stationary. Eventually the core becomes unstable, and the sink starts to accrete matter, marking the formation of the protostar and the start of the Class 0 phase. At this stage the core radius is $\sim 0.05 \text{ pc}$. A freefall velocity field then develops, as material accretes onto the protostar (fourth and fifth rows of Fig. 2). The accretion rate reaches a maximum of $\sim 1.08 \times 10^{-5} M_\odot \text{ yr}^{-1}$, and then declines monotonically (second row of Fig. 7).

In Figure 3 we show results for $\phi = 1$. Here the pressure doubles in one sound-crossing time, and so the evolution is more dynamic (than in the $\phi = 10$ and $\phi = 3$ cases described above). A small compression wave is driven into the core increasing the density and leaving in its wake a modest inward velocity field in the range $(0.10, 0.15) \text{ km s}^{-1}$. The prestellar phase ends – and the Class 0 phase begins – when this compression wave impinges on the centre. Up until this stage, the central density has hardly changed, since the inner parts have been unaware of the increased external pressure; the radius of the core has decreased to $\sim 0.045 \text{ pc}$. During the Class 0 phase, a freefall velocity field develops around the central protostar, but the outer parts of the envelope are

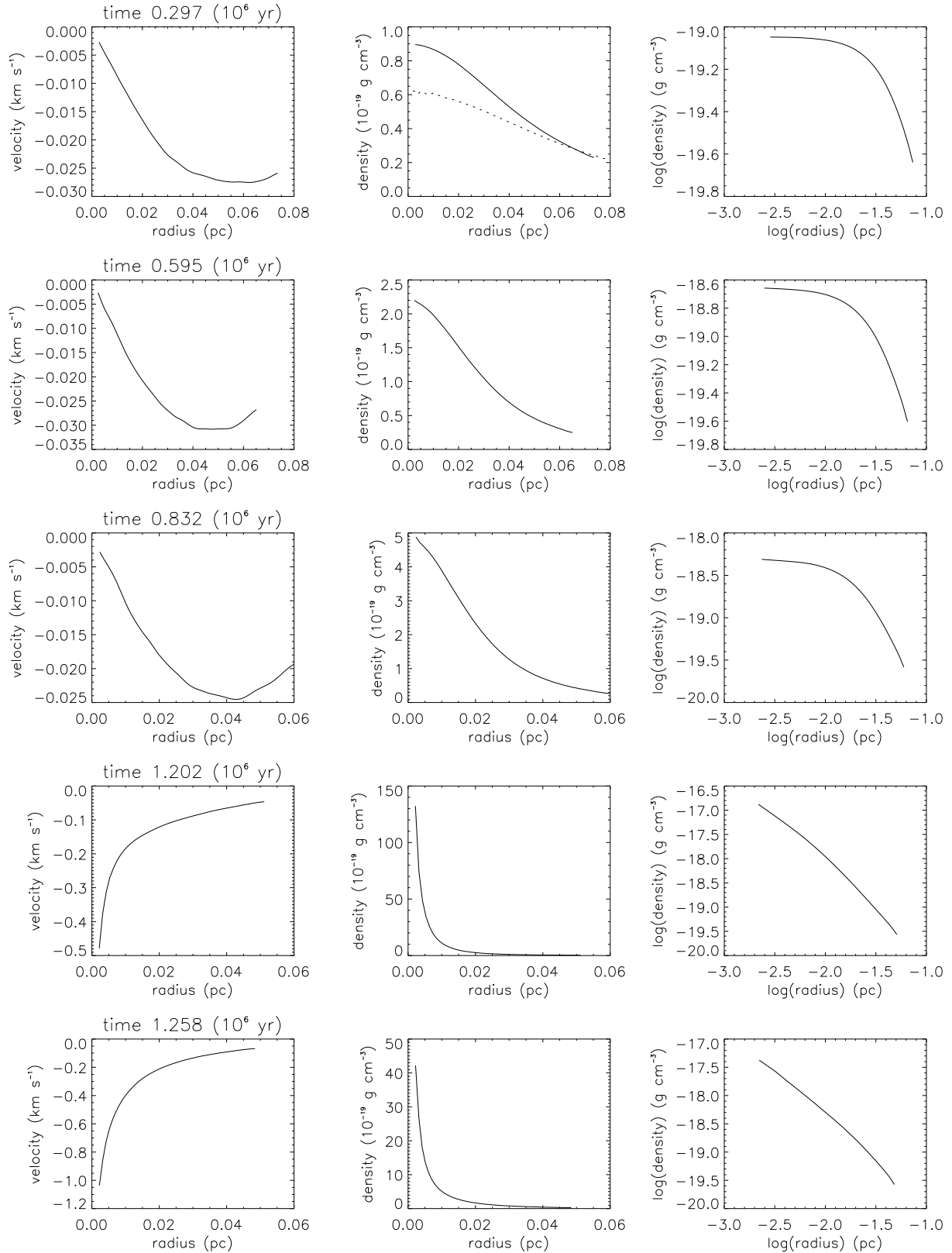


Figure 1. The lefthand column shows velocity profiles on a linear-linear scale, the central column shows density profiles on a linear-linear scale, and the righthand column shows density profiles on a log-log scale, for the case $\phi = 10.0$ (very subsonic compression), at three times during the prestellar phase and two in the Class 0 phase: first row, $t = 0.30$ Myrs; second row, $t = 0.60$ Myrs; third row, $t = 0.83$ Myrs; fourth row, $t = 1.20$ Myrs; fifth row, $t = 1.26$ Myrs. The dashed curve in the first row represents the initial state. We note that with cosmic abundances, a mass density $\rho = 10^{-19} \text{ g cm}^{-3}$ corresponds to a number density $n_H = 2.2 \times 10^{-4} \text{ cm}^{-3}$.

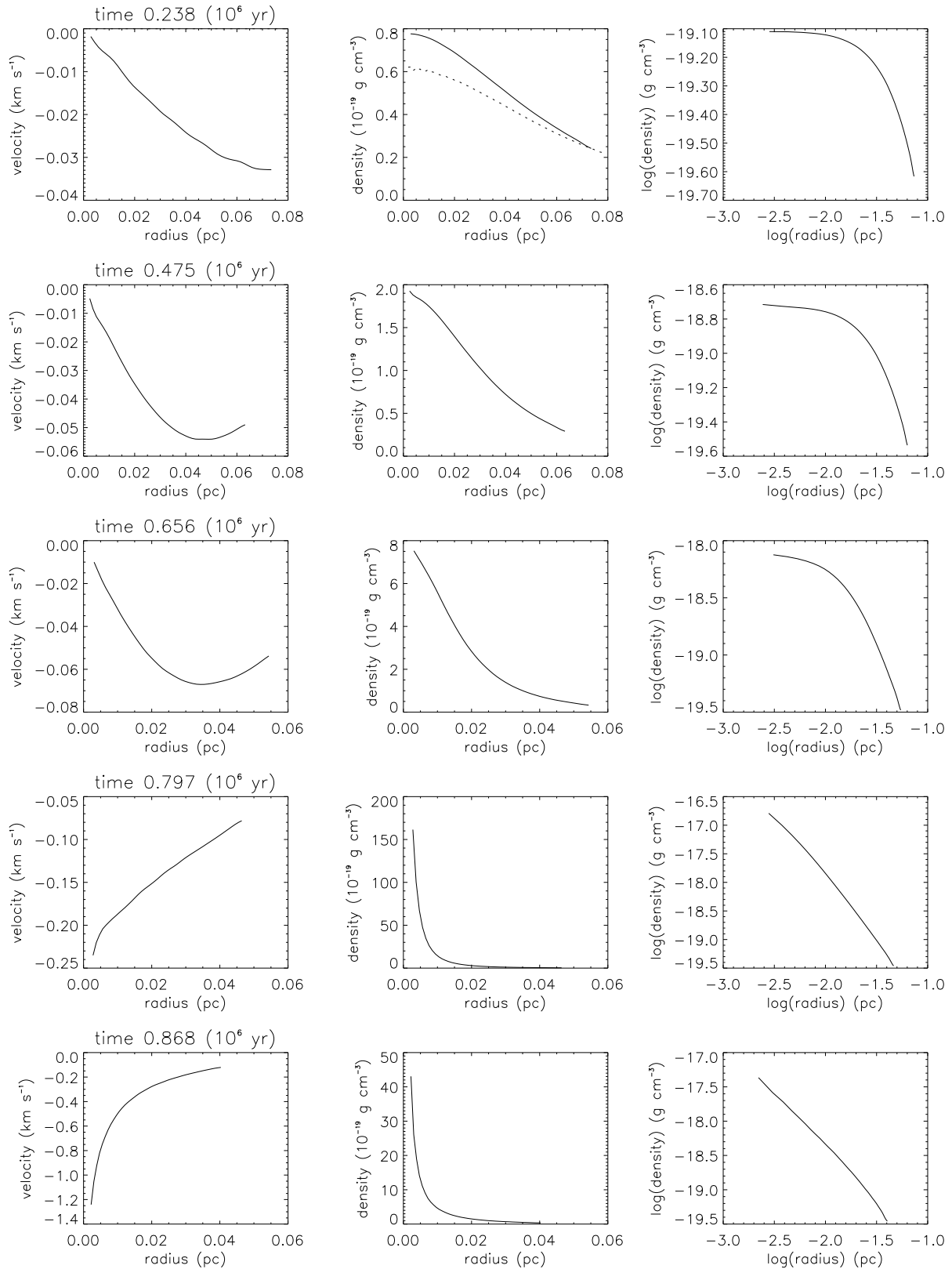


Figure 2. As for Fig. 1, but for the case $\phi = 3.0$ (subsonic compression): first row, $t = 0.24$ Myrs; second row, $t = 0.48$ Myrs; third row, $t = 0.66$ Myrs; fourth row, $t = 0.80$ Myrs; fifth row, $t = 0.87$ Myrs.

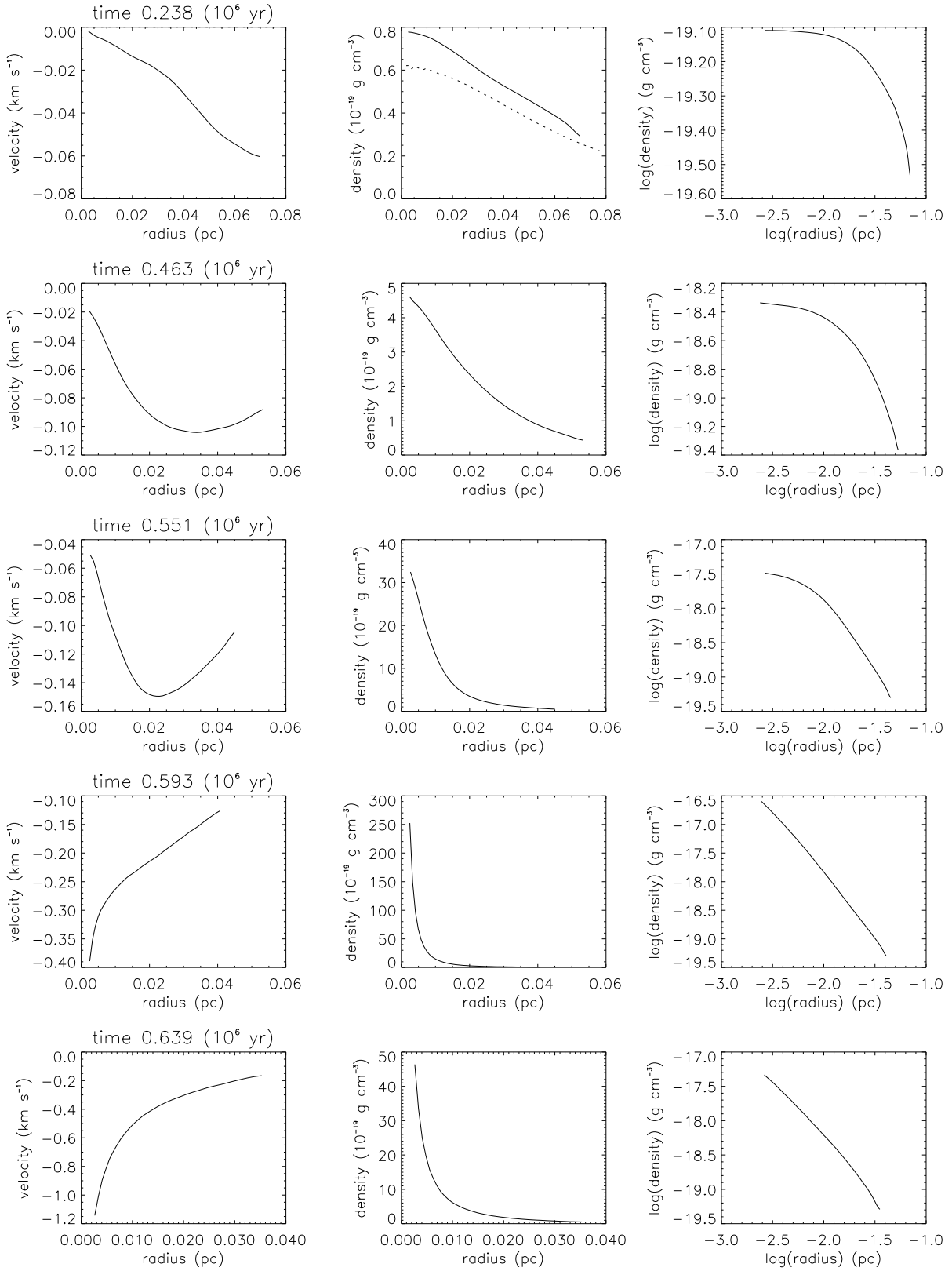


Figure 3. As for Fig. 1, but for the case $\phi = 1.0$ (approximately sonic compression): first row, $t = 0.24$ Myrs; second row, $t = 0.46$ Myrs; third row, $t = 0.55$ Myrs; fourth row, $t = 0.59$ Myrs; fifth row, $t = 0.64$ Myrs.

still moving inwards at approximately uniform sonic speed ($v \sim 0.12 \text{ km s}^{-1}$). The accretion rate is significantly higher than for the more quasistatic cases (larger ϕ), reaching a maximum of $\sim 1.50 \times 10^{-5} M_{\odot} \text{ yr}^{-1}$, and then decreasing into the Class I phase (third row of Fig. 7).

Figure 4 shows detailed results for the case $\phi = 0.3$, i.e. quite rapid compression. In this case a strong compression wave is driven into the core, leaving a marginally *subsonic* velocity field in its wake, i.e. v in the range (0.12, 0.14) km s^{-1} . This leads to quite rapid accretion during the Class 0 phase, reaching a maximum of $\sim 1.65 \times 10^{-5} M_{\odot} \text{ yr}^{-1}$, and then decreasing into the Class I phase (fourth and fifth rows of Fig. 7).

Figure 5 shows detailed results for the case $\phi = 0.1$, i.e. very rapid compression. In this case a very strong compression wave is driven into the core, leaving a mildly *supersonic* velocity field in its wake, i.e. v in the range (0.25, 0.30) km s^{-1} . At $t = 0.24 \text{ Myr}$, the outer layers have been swept up into a *tsunami*. The density at the head of the *tsunami* is ~ 3 times higher than at the centre. This leads to very rapid accretion during the Class 0 phase, reaching a maximum of $\sim 2.60 \times 10^{-5} M_{\odot} \text{ yr}^{-1}$, and then decreasing into the Class I phase (fifth row of Fig. 7). In the Class 0 phase, a freefall velocity field develops in the centre, whilst the outer layers continue to cruise inwards at $v \sim 0.30 \text{ km s}^{-1}$.

If the external pressure only increases for a finite time, and then stays constant at a new higher value, the results are somewhat changed, particularly for the cases of rapid compression (small ϕ). This is illustrated on Fig. 6, where we show detailed results for the $\phi = 0.1$ case when the pressure increase is halted as soon as the pressure has doubled. We refer to this case as “ $\phi = 0.1$ (finite)”, to distinguish it from the standard case “ $\phi = 0.1$ (indefinite)”. In the case “ $\phi = 0.1$ (finite)”, the compression wave is much weaker and slower than for the case “ $\phi = 0.1$ (indefinite)”, and so the inward velocity field it engenders is also weaker. In fact, the evolution for case “ $\phi = 0.1$ (finite)” is more like that for the case “ $\phi = 0.3$ (indefinite)”; in particular, the compression wave takes a comparable time to converge onto the centre. For this reason, the mass and accretion rate for the case “ $\phi = 0.1$ (finite)” are displayed with dashed lines on the same plot as the results for the case “ $\phi = 0.3$ (indefinite)” (i.e. the fourth row of Fig. 7). For slower compression rates, $\phi \gtrsim 1$, halting the pressure increase when the pressure has doubled has little effect, because instability is triggered before the pressure doubles, and the collapse dynamics of the core are therefore already well established.

To test for convergence, we have repeated the case “ $\phi = 1$ (indefinite)” with only $N_{\text{int}} = 20,000$ particles in the core. The time-dependence of the protostellar mass and accretion rate are shown on the third row of Fig. 7 with dotted lines. We see that there is almost no change, except that with fewer particles the compression wave takes a little longer to converge on the centre, about 3% longer. We do not know the reason for this, but in any case it is a very small effect. Apart from this time delay, the detailed density and velocity profiles are essentially unchanged.

Figure 7 shows the accretion rate onto the sink, as a function of time, for the various values of ϕ . The star indicates where the Class 0 phase gives way to the Class I phase. Table 1 shows the durations of the prestellar and

Table 1. The durations of the prestellar and Class 0 phases ($\Delta t_{\text{prestellar}}$ and Δt_{Class0}), and the mean magnitude of the inward velocity field set up during the prestellar phase phases, \bar{v}_{cruise} , for different values of ϕ .

ϕ	$\Delta t_{\text{prestellar}}$ (Myrs)	Δt_{Class0} (Myrs)	\bar{v}_{cruise} (km s^{-1})
10.0	1.2	0.11	0.025
3.0	0.8	0.05	0.06
1.0	0.6	0.04	0.12
0.3	0.4	0.03	0.17
0.1	0.3	0.02	0.30

Class 0 phases, for representative values of ϕ . Since the sink particle is present from the outset, the moment of protostar formation is not precisely defined, and therefore these durations are not precisely defined. They simply illustrate the fact that the prestellar and Class 0 phases are accelerated by rapid compression. In all cases, $\Delta t_{\text{Class0}}/\Delta t_{\text{prestellar}} \sim 0.05$ to 0.10 .

We also tabulate values of \bar{v}_{cruise} , which is the mean inward velocity established in the outer parts of the core as a result of the passage of the inward propagating compression wave. These values are obtained from the detailed velocity profiles by inspection, and are therefore only indicative of the general trend. The inward velocities observed in the outer envelopes of isolated prestellar cores in nearby star formation regions range from $\sim 0.04 \text{ km s}^{-1}$ to $\sim 0.10 \text{ km s}^{-1}$ (Lee, Myers & Tafalla 1999). Our models generate comparable velocities for ϕ in the range (1, 10), i.e. for situations in which the external pressure increases on a time-scale comparable with or greater than the sound-crossing time.

We speculate that collapses with lower values of ϕ , i.e. more dynamical collapses, arise in more violently triggered star formation regions such as the ρ Ophiuchi and Perseus protoclusters (cf. Motte & André 2001). This would explain their having higher absolute densities and smaller extents at the onset of the Class 0 phase.

4 DISCUSSION

The obvious inference to be made from these simulations is the unsurprising one that, the more rapid and the more prolonged the increase in external pressure, the more rapid is the evolution, the stronger is the compression wave, the higher is the peak accretion rate, and the shorter are the prestellar and Class 0 phases. However, other important inferences are to be found in the detail. In particular, simulations with $\phi \gtrsim 1$ (i.e. pressure increasing on a sound-crossing time or slower) match essentially all the observational constraints described in Section 2.

First, the density profiles in the prestellar phase are relatively flat in the inner regions, $\eta \equiv -d \ln[\rho]/d \ln[r] \lesssim 1$, and steepen towards $\eta \sim 2$ in the outer parts. The effect of the compression wave will be hard to detect in projection. It will simply produce an apparent extension of the relatively flat inner part of a prestellar core. By the Class 0 and Class I phases, the density profiles should steepen, viz. to $\eta \sim 3/2$ in the inner regions, and to $\eta \sim 2 - 3$ in the outermost regions (see log-log plots of the density at late times in Figs. 1 to 5).

Second, the velocity fields are very reminiscent of that

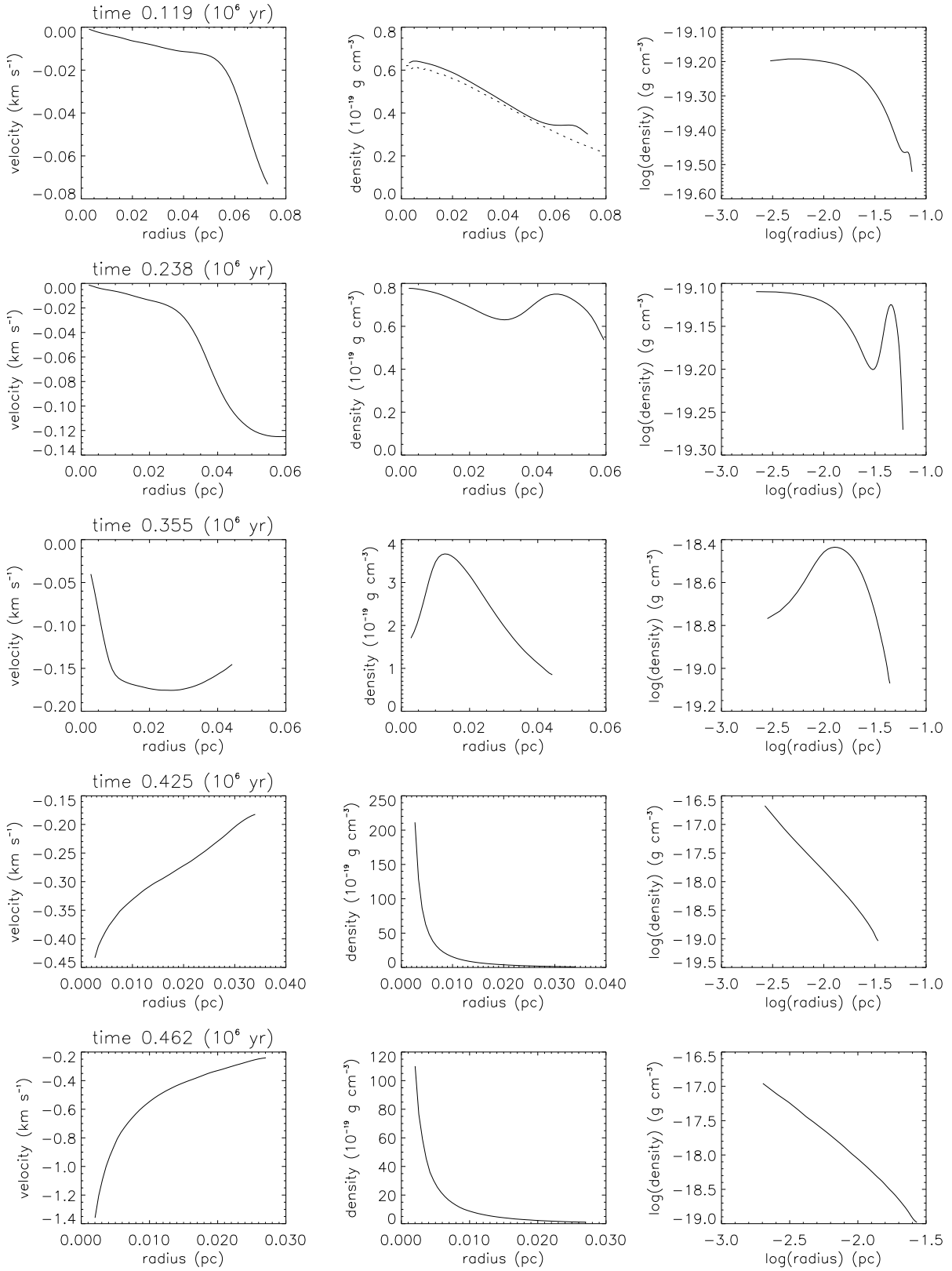


Figure 4. As for Fig. 1, but for the case $\phi = 0.3$ (mildly supersonic compression): first row, $t = 0.12$ Myrs; second row, $t = 0.24$ Myrs; third row, $t = 0.36$ Myrs; fourth row, $t = 0.43$ Myrs; fifth row, $t = 0.46$ Myrs.

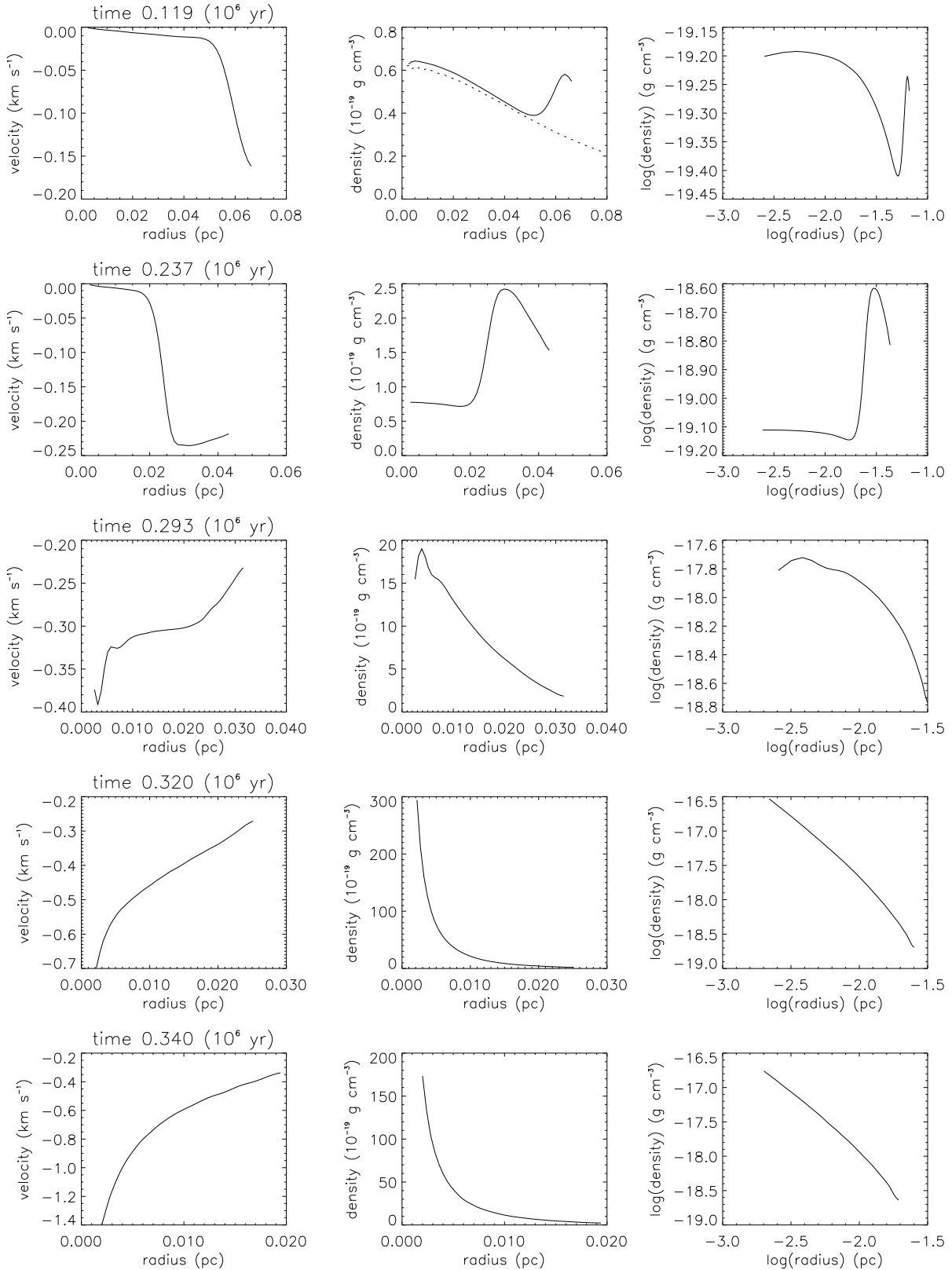


Figure 5. As for Fig. 1, but for the case $\phi = 0.1$: first row, $t = 0.12$ Myrs; second row, $t = 0.24$ Myrs; third row, $t = 0.29$ Myrs; fourth row, $t = 0.32$ Myrs; fifth row, $t = 0.34$ Myrs.

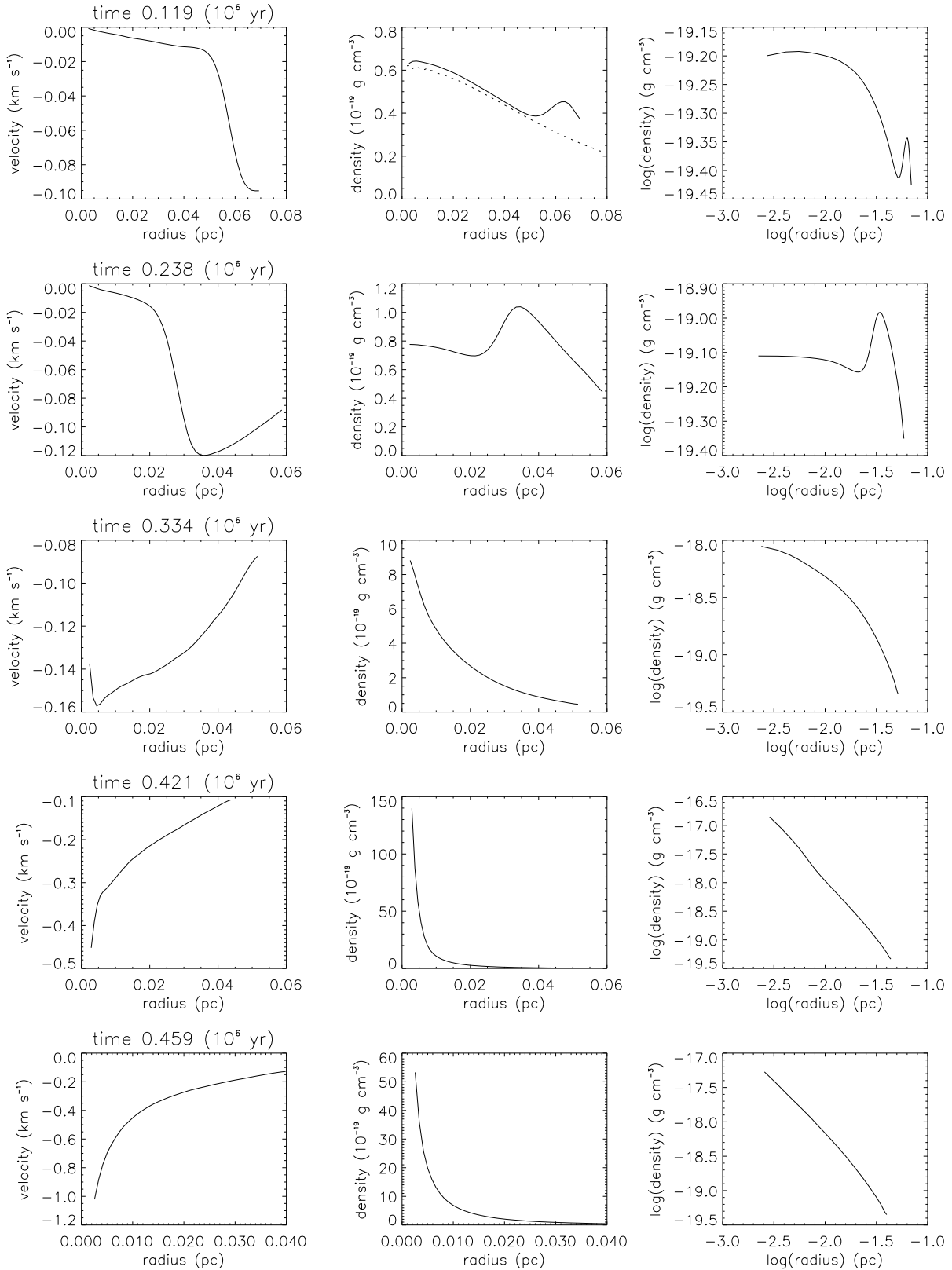


Figure 6. As for Fig. 1, but for the case $\phi = 0.1$ (finite), where instead of letting P_{ext} increase indefinitely, the increase is halted once P_{ext} has doubled: first row, $t = 0.12$ Myrs; second row, $t = 0.24$ Myrs; third row, $t = 0.33$ Myrs; fourth row, $t = 0.42$ Myrs; fifth row, $t = 0.46$ Myrs.

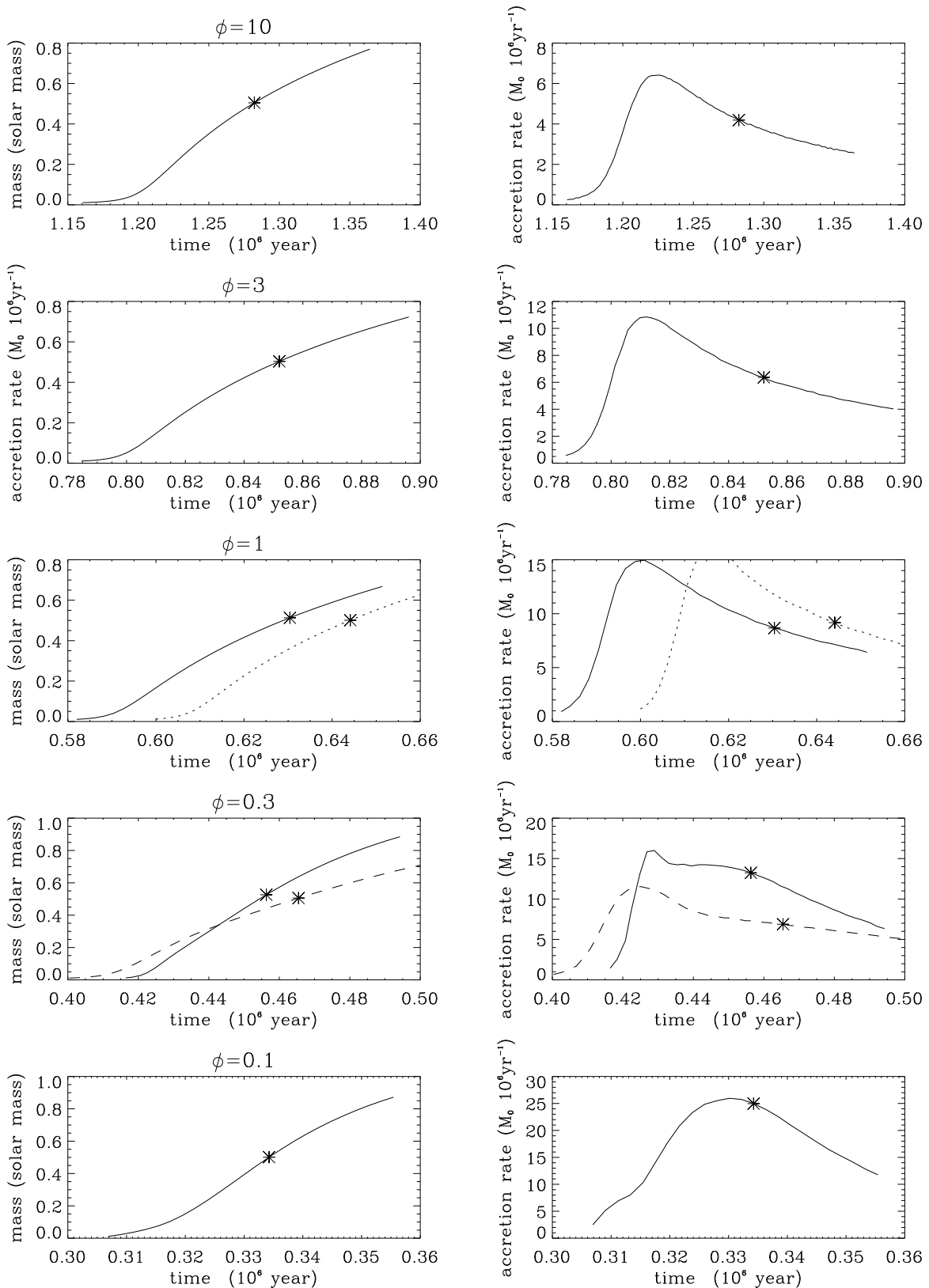


Figure 7. Accretion rates as a function of time. First row, $\phi = 10$; second row, $\phi = 3$; third row, $\phi = 1$; fourth row, $\phi = 0.3$; fifth row, $\phi = 0.1$. The full curves correspond to the standard simulations, i.e. those in which P_{ext} is allowed to increase indefinitely. The dotted curves on the third row correspond to the “ $\phi = 1$ (indefinite)” case, but performed with fewer particles (i.e. $N_{\text{int}} = 20,000$ instead of the standard $N_{\text{int}} = 50,000$) in the core. The dashed curves on the fourth row correspond to the case $\phi = 0.1$ (very fast compression), but where P_{ext} is held constant once it has doubled, i.e. “ $\phi = 0.1$ (finite)”. It is plotted with the $\phi = 0.2$ (indefinite)” case on the fourth row.

inferred for L1544 by Tafalla et al. (1998) and Williams et al. (1999). In L1544 the velocity field in the outer parts of the core appears to be approximately uniform, with magnitude $\sim 0.08 \text{ km s}^{-1}$. Other cores showing similar infall signatures give inward velocities in the range $\sim 0.04 \text{ km s}^{-1}$ to $\sim 0.10 \text{ km s}^{-1}$ (Lee, Myers & Tafalla 1999). If these velocities are due to an inward-driven compression wave of the type we have simulated, it suggests that the external pressure increases on a time-scale comparable with, but somewhat greater than, a sound-crossing time.

The generation of an approximately uniform inward radial velocity field appears to be a generic feature of compression waves. All of the two-dimensional infinity of similarity solutions found by Whitworth & Summers (1985) involve compression waves which are driven from the outside inwards, and which leave behind them a uniform inward velocity field ($v_{\text{rad}} \simeq \text{constant}$) and a $\rho \propto r^{-2}$ density field. The convergence of this compression wave on the centre at $t = 0$ signals the formation of a central stellar object. This object then grows at a constant accretion rate. At the same time an expansion wave is reflected outwards and leaves in its wake an approximately freefall velocity field, $v_{\text{rad}} \propto r^{-1/2}$, and $\rho \propto r^{-3/2}$. The Shu (1977) solution is simply the limiting case of a zero-amplitude compression wave leaving a zero-amplitude inward velocity field in its wake; hence, uniquely, it starts from a static singular isothermal sphere. The Larson-Penston solution involves a fairly strong compression wave propagating into a uniform-density, homologously contracting cloud. If radial velocity fields like that inferred for L1544 turn out to be common, one possible explanation is that core collapse and protostar formation generally follow from external compression.

Third, the accretion rate is very high immediately after the formation of the central protostar, i.e. in the Class 0 phase, but later it decreases. This conforms to the pattern of accretion inferred from the decline in outflow power between the Class 0 and the Class I phase (Bontemps et al. 1996, Henriksen et al. 1997), and is consistent with the relative numbers of Class 0 and Class I sources.

A rapid increase of external pressure, of the sort we have invoked in these simulations, could arise in a number of situations. In the first instance, we might presuppose the existence of an approximately stable gravitationally bound core. If this core were then overrun by a strong shock which propagated supersonically through the medium surrounding the core, the external pressure acting on the core boundary would be increased. Alternatively, if the medium surrounding the core were suddenly irradiated more intensely, because a luminous star switched on nearby, or came out from behind a dust cloud, the surrounding medium would be heated – and possibly also ionized – giving a rapid increase in the external pressure. A contraction of the molecular cloud in which the core is embedded, as in the scenario of Palla & Stahler (2000), would also lead to an increase (presumably slow) in the external pressure bounding the dense core. A similar type of collapse would ensue if the radiation heating the core were suddenly shut off (but not that heating the external medium). The core would become thermally unstable, and the external medium would drive in a compression wave. It is also possible that the same convergent flows which create cores in the first place, may sometimes then continue to compress these cores until they collapse, as

in the scheme recently described by Hartmann, Ballesteros-Paredes & Bergin (2001).

However, it is very unlikely that the increase in the external pressure would actually be isotropic – as we have assumed, for simplicity, in the simulations presented here. Therefore we should not expect compression waves to converge on the centre simultaneously from all directions. Instead, the compression waves arriving from different directions are likely to be out of phase, so that they will interfere in complex ways. This could have the effect of creating multiple protostellar seeds in the interior of a core, in accordance with the observation that most stars are born in binary or higher multiple systems (Mathieu 1994).

5 CONCLUSIONS

We conclude that the model of protostellar collapse developed here merits further investigation. It appears to reproduce the gross features of the density and velocity fields observed in prestellar cores and protostars, and the relative ages of the Class 0 and Class I phases. We now need to explore the consequences of introducing an energy equation, the effect of initial rotation, and the influence of perturbations as a means of inducing the formation of binaries and higher multiples.

ACKNOWLEDGEMENTS

PH, APW, and PhA gratefully acknowledge the support of an European Commission Research Training Network under the Fifth Framework Programme (No. HPRN-CT2000-00155), and useful discussions with Derek Ward-Thompson, Arnaud Belloche and Pierre Lesaffre. PPG gratefully acknowledges the support of a PPARC postgraduate studentship.

REFERENCES

- Abergel A., et al., 1996, *A&A*, 315, L329
- André P., Montmerle T. 1994, *ApJ*, 420, 837
- André P., Ward-Thompson D., Barsony M., 1993, *ApJ*, 406, 122
- André P., Ward-Thompson D., Barsony M., 2000, in *Protostars and Planets IV*, eds. V. Mannings, A.P. Boss, & S.S. Russell (Univ. of Arizona Press, Tucson), p. 59
- Bacmann A., André P., Puget J.-L., Abergel A., Bontemps S., Ward-Thompson D., 2000, *A&A*, 361, 555
- Barnes J., Hut P., 1986, *Nature*, 324, 446
- Bate M. R., Burkert A., 1997, *MNRAS*, 288, 1060
- Beichman C. A., Myers P. C., Emerson J. P., Harris S., Mathieu R., Benson P. J., Jennings R. E., 1986, *ApJ*, 307, 337
- Benson P. J., Myers P. C., 1989, *ApJS*, 71, 89
- Bonnor W.B., *MNRAS*, 116, 351
- Bontemps S., André P., Terebey S., Cabrit S., 1996, *A&A*, 311, 858
- Bourke T. L., Hyland A. R., Robinson G., 1995, *MNRAS*, 276, 1052
- Clemens D. P., Barvainis R., 1988, *ApJS*, 68, 257
- Evans N. J. II, Rawlings J. M. C., Shirley Y. L., Mundy L. G., 2001, *ApJ*, 557, 193
- Foster P. N. & Chevalier R. A., 1993, *ApJ*, 416, 303
- Greene, T.P., Wilking, B.A., André, P., Young, E.T., & Lada, C.J. 1994, *ApJ*, 434, 614

- Gregersen E. M., Evans N. J. III, 2000, *ApJ*, 538, 260
Hartmann L. W., Ballesteros-Paredes J., Bergin E. A., 2001, *ApJ*, 562, 852
Henriksen, R. N., André P., Bontemps S. 1997, *A&A*, 323, 549
Hernquist L., 1987, *ApJS*, 64, 715
Jessop N. E., Ward-Thompson D., 2000, *MNRAS*, 311, 63
Jessop N. E., Ward-Thompson D., 2001, *MNRAS*, 323, 1025
Kenyon S. J., Hartmann L. W., 1995, *ApJS*, 101, 117
Lada C. J., 1987, in Peimbert M., Jugaku J., IAU Symposium 115, Star Forming Regions, p.1. Reidel, Dordrecht
Lada C. J., Wilking B., 1984, *ApJ*, 287, 610
Lee C. W., Myers P. C., 1999, *ApJS*, 123, 233
Lee C. W., Myers P. C., Tafalla M., 1999, *ApJ*, 526, 788
Mathieu, R. D. 1994, *ARA&A*, 32, 465
Monaghan J. J., Lattanzio J. C., 1985, *A&A*, 149, 135
Motte F. & André P., 2001, *A&A*, 365, 440
Myers P. C., Benson P. J., 1983, *ApJ*, 266, 309
Myers P. C., Lazarian A., 1998, *ApJ*, 507, L157
Myers P. C., Evans N. J., Ohashi N., 2000, in *Protostars and Planets IV*, eds. V. Mannings, A.P. Boss, & S.S. Russell (Univ. of Arizona Press, Tucson), p. 217
Palla F., Stahler S. W. 2000, *ApJ*, 540, 255
Shu F. H., 1977, *ApJ*, 214, 488
Stahler S.W., Walker F.M., 1993, in *Protostars and Planets III*, eds. V. Mannings, A.P. Boss, & S.S. Russell (Univ. of Arizona Press, Tucson), p. 405
Shu F. H., Adams F. C., Lizano S., 1987, *ARA&A*, 25, 23
Tafalla M., Mardones D., Myers P. C., Caselli P., Bachiller R., Benson P. J., 1998, *ApJ*, 504, 900
Turner J. A., Chapman S. J., Bhattal A. S., Disney M. J., Pongracic H., Whitworth A. P., 1995, *MNRAS*, 277, 705
Ward-Thompson D., André P., Kirk, J. M., 2001, *MNRAS*, in press
Ward-Thompson D., Motte F., André P., 1999, *MNRAS*, 305, 143
Ward-Thompson D., Scott P. F., Hills R. E., André P., 1994, *MNRAS*, 268, 276
Whitworth A. P., Summers D., 1985, *MNRAS*, 214, 1
Whitworth A. P., Ward-Thompson D., 2001, *ApJ*, 547, 317
Williams J. P., Myers P. C., Wilner D. J., Di Francesco J., 1999, *ApJ*, 513, L61
Zucconi A., Walmsley C. M., Galli D., 2001, *A&A*, 376, 650

This paper has been produced using the Royal Astronomical Society/Blackwell Science \LaTeX style file.